A numerical study of the impurity effects on CO_2 geological storage in layered formation

Didi Li [a], Yao He [a], Hongcheng Zhang [a], Wenbin Xu [a,*], Xi Jiang [b,*]

[a]*School of Environmental Science and Engineering, Guangdong University of Technology, Guangzhou, China*
[b]*School of Engineering and Materials Science, Queen Mary University of London, Mile End Road, London E1 4NS, UK*

Abstract

The effects of two kinds of common impurities (*i.e.*, N_2 and H_2S) on CO_2 geological storage in layered formations were investigated by numerical simulations. This study was focused on the migration behaviour and spatial distribution of CO_2 plume. The effects of capillary pressure on the spread of CO_2 plume in the layered formations were examined first. The results suggested that the capillary pressure was a minor influence when injecting, but it affected the migration and distribution of CO_2 plume significantly during post-injection period in which, the contact area between CO_2 plume and formation brine became smaller with increased capillary pressure, leading to a decrease of dissolved CO_2 mass fraction. In the case of co-injection of CO_2 with N_2 impurity, it was found that as the N_2 concentration rose up, the horizontal migration distance of CO_2 plume extended, and the plume inclined to accumulate below the impermeable caprock. The phenomena were due to the enhancement of buoyance effect of CO_2 plume and accordingly, the contact area between the CO_2 plume and the formation brine enlarged, resulting in an increase of dissolved CO_2 mass fraction. However, the effects of H_2S impurity were less obvious compared with N_2, and only a little shrinkage of the distribution range of CO_2 plume could be observed when H_2S was co-injected.

Keywords: Layered formation; Impurity; Carbon capture and storage; Numercal simulation.

1. Introduction

Carbon capture and storage (CCS) has been regarded as one of the most promising technologies to reduce CO_2 concentrations in the atmosphere [1-3]. Among various potential storage options, CO_2 storage in geological formations such as deep saline aquifers is considered as the most effective method in the short-to-medium term [2]. The geological formations suitable for CO_2 storage are usually below 800 m, where CO_2 may exist in the supercritical form (the supercritical fluid is sometimes referred to as "gas" for simplicity and easier reference) and its density ranges from 50% to 80% of that of water [1]. Under these conditions, CO_2 will migrate upwards due to buoyancy effects until it is blocked by impermeable caprock [2]. Most potential formations suitable for CO_2 storage are stratified, which means that the geological formations are composed of a number of alternating high-permeability and low-permeability layers, such as sands and shales. For example, the formations of the storage site at Sleipner, Norway are layered, with low-permeability shale layers embedded in high-permeability sand layers. Although these low-permeability layers may not be tight enough to prevent the upward movement of most CO_2 [4], these layers play an important role in preventing CO_2 leakage as there might be unexpected faults in the caprock [5-8]. Using the geological conditions at Sleipner, numerical simulations have been carried out to investigate the distribution and evolution of the CO_2 plume as well as the dissolved CO_2 concentration [9,10]. Their results confirmed that the ascent rate of the plume was limited by these low-permeability layers. More importantly, based on the same model, they compared the results of different software packages. Predictions for shape and growth of the CO_2 plume showed good agreement, which gives much confidence to the model.

Currently, different aspects of CO_2 storage in stratified formations have been investigated including the pressure response to CO_2 injection. By numerical simulation, it was found that the pressure buildup was considerably large when a single injection site was used in a large sedimentary multilayered formation [11].

* Corresponding author. Tel.: +44-20-7882 5009.
E-mail address: xi.jiang@qmul.ac.uk; qmwxjiang@outlook.com
* Corresponding author. Tel.: +86-133-1883-1883.
E-mail address: xuwenbin@gdut.edu.cn; 13318831883@163.com

An analytical solution was also developed and demonstrated to be efficient for the prediction of the pressure buildup in the corresponding stratified system [12,13]. Li et al. suggested that injection through multiple layers is preferable for these basin-scale sites to increase the injectivity and storage efficiency, and to reduce the risk of overpressure [14]. Simulation results of a multilayer injection in Shenhua CCS demonstration project in China showed a much wider range of the pressure perturbation compared with that of the supercritical CO_2 plume [15]. Different injection schemes for layered reservoirs were investigated and compared to find a balance between economic benefit and trapping efficiency [16]. Besides, the ambient mudrocks were suggested to influence both the lateral and vertical pressure evolution in layered system [17].

It should be noted that the model adopted can influence the simulation results. Liu and Zhang [18] compared the results of three stratigraphic models (*i.e.*, facies, layered and formation) with that of detailed heterogeneous models and found that the layered model was optimal for predicting gas flow and storage. Although the pressure response obtained by a simple one-layer and a refined multi-layer model was similar, the plume spread in the refined multi-layer model was larger [19]. Figueiredo et al. pointed out that an equivalent single-layer formation was inadequate to substitute a three-layer formation due to the significant differences in the spread of CO_2 plume [20].

Investigations related to the impact of many parameters on the morphology of CO_2 plume have also been documented. For example, the injection rate was suggested to be the dominant factor controlling both the upward and outward movement of the CO_2 plume from an injection point, and specifically, a higher rate could facilitate the vertical penetration of CO_2 through the thin low-permeability layers [21]. The distribution of CO_2 saturation in low-permeability layers was shown to be more sensitive to the injection rate than that in high-permeability layers, which suggests that an increase of the injection rate would more effectively improve the storage capacity in low-permeability layers [22]. Well placements in stratified formations were found to impact total amount of CO_2 sequestrated in the geological formations [23]. Moreover, different layering sequences resulted in distinct evolution of the gas phase [24]. Kano and Ishido pointed out that the thickness of alternating sandstone and shale layers had rather large impact on the distribution of the supercritical plume and the long-term behavior of CO_2 [25]. Cavanagh and Haszeldine suggested that the threshold pressures of shale layers were responsible for the pattern of multiple thin layers of CO_2 within the Utsira Formation [26]. Sung et al. conducted a field scale simulation and suggested that the sloping of stratified formations had a significant effect on the migration behaviours of CO_2 plume [27].

Injected CO_2 will gradually dissolve in the formation brine that makes it safer than CO_2 in supercritical mobile form [28], and this is known as the solubility trapping mechanism. The multilayer property of the storage formation also affects this mechanism [29]. It is suggested that the layering of aquifer storage formation increased the dissolution rate of CO_2 because the two-phase contact area was larger [30]. In the low-permeability layer in stratified systems, in spite of the fact that the dominant mixing mechanism may be the diffusive mixing process instead of the much faster convective mixing process, the horizontal distribution of the plume spread under low-permeability layers increased the contact area and thus the dissolved CO_2 mass [31].

Although CO_2 storage in layered formations has been investigated extensively, the studies rarely take impurities into consideration. As a matter of fact, no matter which capture technology is adopted, the captured CO_2 streams always contain a proportion of non-CO_2 species, such as N_2, O_2, Ar, H_2S, SO_2, etc. [32-34]. Since purity requirements significantly increase the total cost of CCS, most CCS projects employ impure CO_2. However, impurities will influence CO_2 storage security and effectiveness due to their distinctly different properties from that of CO_2 [e.g., 34-40]. It is thus necessary to investigate the coupling effects of multilayered formation and impurity on CO_2 storage to obtain a better understanding of CCS. In the present study, numerical simulations were carried out to investigate the effects of capillary pressure and two common impurities, N_2 and H_2S, on CO_2 storage in stratified formations. Three aspects were mainly considered: (1) The evolution of the spatial distribution of CO_2 plume; (2) The distribution of CO_2 and impurity in the supercritical plume, including the partitioning phenomenon between CO_2 and the co-injected impurity; (3) Phase partition of CO_2 in the aqueous and non-aqueous phases. The study is expected to provide insights on the effects of impurities on geological carbon storage in multilayered formations, which can help the deployment of CCS technology.

2. Physical model

This study is patterned after the CO_2 injection project in Utsira Formation at the Vest field of Sleipner. Many features of the actual injection are captured, including the geometry and permeability of the host formation. However, in order to make a tractable problem, some simplifications have been made, including the assumption of isothermal conditions and the simplification of permeability details in the real situation [9,10]. As shown in Figure 1, it is a symmetric two-dimensional model, with the height of 184 m and width of 6000 m. Four layers of low-permeability shale are distributed in the high-permeability sand layers. The horizontal injection well is located 30 m beneath the fourth shale layer. Both the top and bottom boundaries are impermeable. The left boundary permits no flux through it while the right boundary condition is hydrostatic pressure, preventing possible overpressure of the formation. In the present study, the compositional reservoir simulator CMG-GEM [41] is adopted to carry out the computational simulations. The fluid properties and the model parameters are listed in Table 1. The correlations of relative permeability and capillary pressure are the same as those in the simulations of Pruess et al. [10].

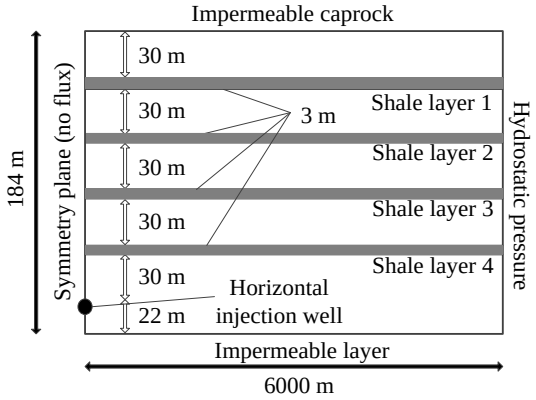

Fig. 1. Schematic representation of the geometry in Utsira Formation [10].

The permeability and porosity of the formations are usually determined by practical measurement, while the capillary pressure is often provided by empirical or semi-empirical formula such as the correlation of Van Genuchten [42].

$$p_c = -P_0\left(\left[S^*\right]^{-1/\lambda} - 1\right)^{1-\lambda} \tag{1}$$

where P_0 stands for the intensity factor. In order to evaluate the effect of capillary pressure on the migration and distribution of the supercritical CO_2 plume in layered saline formations, different combinations of the intensity factor in sand and shale layers are adopted in this study, as listed in Table 2. The intensity factors in Case 4 are the same as those in the simulations of Pruess et al. [10].

It should be noted that the injected stream is pure CO_2 in the investigation of the effects of capillary pressure. For the investigation of the effects of impurity, the injected stream is the CO_2-N_2 and CO_2-H_2S mixture respectively, while the capillary pressures are set as the values in Case 4. Since the maximum possible mole fraction of N_2 in most practical CCS operations is 10% [33,43], the upper limit of N_2 concentration is chosen to be 10%. The concentrations of H_2S in the injected CO_2 streams are usually lower than 10%, except for the case of acid gas injections [e.g., 2,38]. However, in order to compare and analyze the effects of these two different impurities at equal concentration, the same initial feed gas compositions are adopted for CO_2-N_2 and CO_2-H_2S mixtures. Furthermore, the impurity mole fractions of 2% and 5% are also chosen in order to evaluate the effects of the variation of impurity concentrations.

Table 1. Fluid properties and model parameters.

Temperature	37 °C
Pressure at well	110 bar
Density of injected CO_2	721.63 kg/m^3
Density of injected N_2	117.79 kg/m^3
Density of injected H_2S	770.67 kg/m^3
Viscosity of injected CO_2	5.8950×10^{-5} Pa·s
Viscosity of injected N_2	2.0530×10^{-5} Pa·s
Viscosity of injected H_2S	1.3516×10^{-4} Pa·s
Salinity	3.2 wt.-%
Sand permeability	3×10^{-12} m^2
Shale permeability	10^{-14} m^2
Sand porosity	0.35
Shale porosity	0.1025
Injection rate	17.23 m^3/day
Injection time	2 years
Simulation time	10 years

Table 2. Cases for the investigations of capillary pressure.

	Case 1	Case 2	Case 3	Case 4
Sand layer P_0 (kPa)	0	3.58	3.58	3.58
Shale layer P_0 (kPa)	0	3.58	31.0	62.0

3. The effects of the capillary pressure

Figure 2 shows the distribution of gas saturation after 2 years' injection for different cases of capillary pressures, with the leading edge of CO_2 plume highlighted. The injected CO_2 plume tends to migrate upwards because its density is lower than that of the formation brine. However, the low-permeability and low-porosity shale layers hinder the rise of CO_2 plume. As a result, the plume accumulates and horizontally migrating away from the injection well under these shale layers. The phenomena are consistent with time-lapse seismic monitoring results that CO_2 would be retained in large thin clouds under the semi-permeable shale layers [4,26,44-47].

Comparing Figure 2a and 2b, it is found that the existence of capillary pressure affect the migration and distribution of the CO_2 plume in layered formations. When the capillary pressures in the sand and shale layers are the same but relatively small (Case 2), the maximum horizontal migration distance of the supercritical plume is less than 1800 m, shorter than that in Case 1 (about 2200 m). The shrinkage of the maximum horizontal migration distance is mainly because the capillary pressure in the sand layers makes it harder for CO_2 to displace the formation brine. Furthermore, the capillary pressure in the shale layers impedes the ascent of the CO_2 plume. As a result, CO_2 that has penetrated through the shale layers is less, resulting in shorter migration distance under shale layers 1-3. On the whole, when capillary pressure is not taken into account, the distribution range of high gas saturation (S_g>0.5) is larger than that in the cases considering capillary pressure.

With the same capillary pressure in the sand layers, the variation of capillary pressure in the shale layers would alter the distribution range of the supercritical plume (from Case 2 to Case 4). When the capillary pressure in the shale layers increases, the upward movement of the CO_2 plume becomes more difficult. As a result, more CO_2 would be retained under shale layer 4 and migrate horizontally farther away. At the meantime, the amount of CO_2 that has ascended through the shale layers decreases, particularly the amount of supercritical CO_2 that has reached and accumulated under the caprock (Figures 2b-d). Anyway, during the injection period, the effects of capillary pressure are insignificant since the main driving force for the migration of the CO_2 stream is the pressure buildup caused by injection.

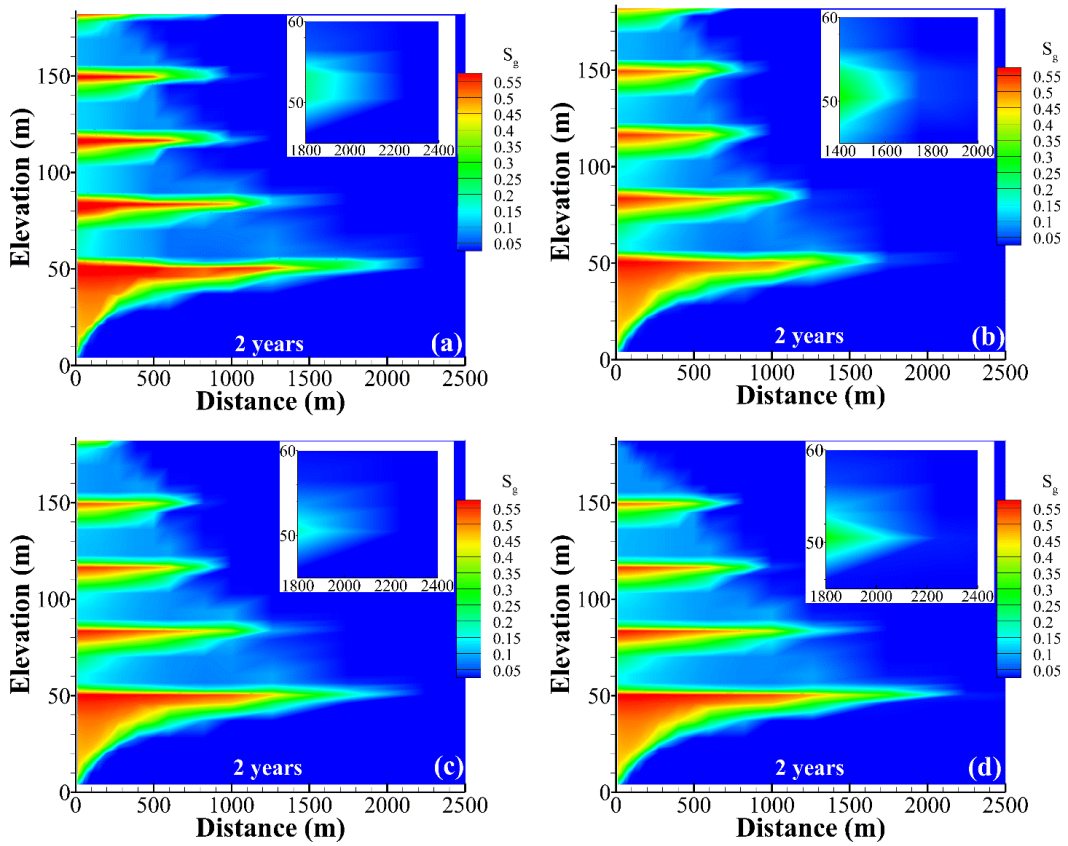

Fig. 2. The distribution of gas saturation after 2 years' injection for different cases of capillary pressures: (a) Case 1; (b) Case 2; (c) Case 3; (d) Case 4.

Figures 3 and 4 illustrate the distribution of gas saturation after 5 years and 10 years, respectively. When the 2 years' injection has stopped, the pressure buildup caused by CO_2 injection decreases gradually. During the first few years of the post-injection period, CO_2 stream continues migrating farther away, but at a rather slow pace. For instance, the leading edge of CO_2 plume in Case 1 only advances 200 m in 3 years after the injection has stopped (Figure 3a). Moreover, the formation brine would backflow during the post-injection period. At the meantime, CO_2 plume continues rising up due to buoyancy effects. As a result, the migration distance of CO_2 under shale layers decreases, while the migration distance of CO_2 under the impermeable caprcok increases considerably. As a matter of fact, with more and more CO_2 accumulating under the caprock, it becomes the leading edge of CO_2 plume (Figure 4a).

When the capillary pressure is relatively small (Case 2), the distribution of gas saturation shares a similar pattern with that in Case 1, except that the migration distance is shorter. By careful examination between Figure 3a and 3b, it is found that difference of the migration distance is less than 300 m after 5 years, while the difference is more than 400 m after 2 years (Figures 2a and 2b). This is because the capillary pressure in the sand layers hinders the backflow of the formation brine during the post-injection period.

The capillary pressure in the shale layers plays an important role in the evolution of the CO_2 plume in layered formations after the injection has stopped. As can be seen in Figures 4c and 4d, instead of shrinking like that in Case 1 or 2, the supercritical CO_2 plume under the shale layers migrates gradually outwards from the injection site during the post-injection period. This is mainly because the relatively large capillary pressure in the shale layers limits the upward moving of the CO_2 plume, and thus more CO_2 is kept under the shale layers. As a consequence, the gas pressure of the remaining CO_2 stream is large enough to keep the stream migrating forwards.

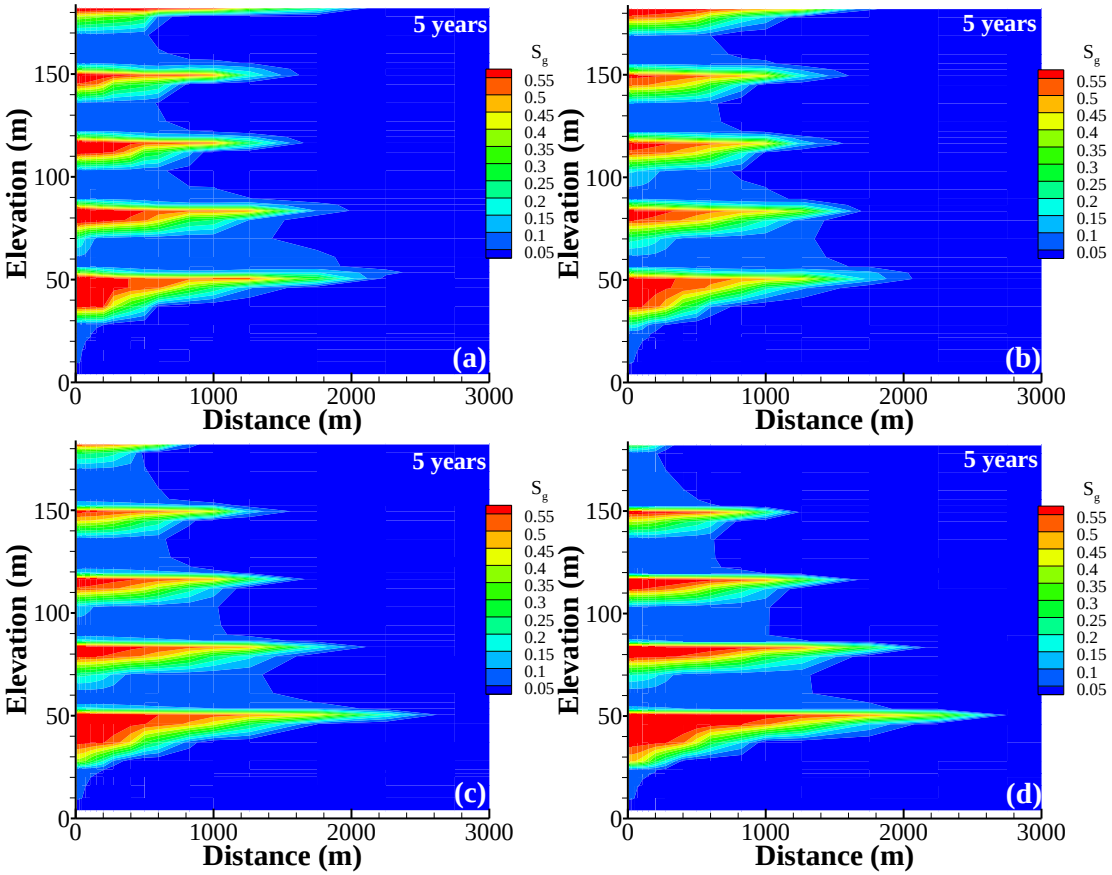

Fig. 3. The distribution of gas saturation after 5 years for different cases of capillary pressures: (a) Case 1; (b) Case 2; (c) Case 3; (d) Case 4.

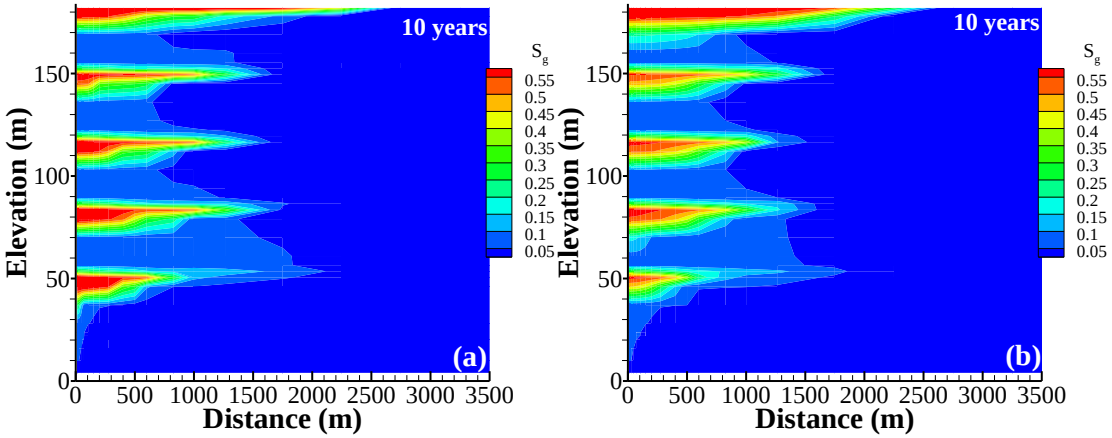

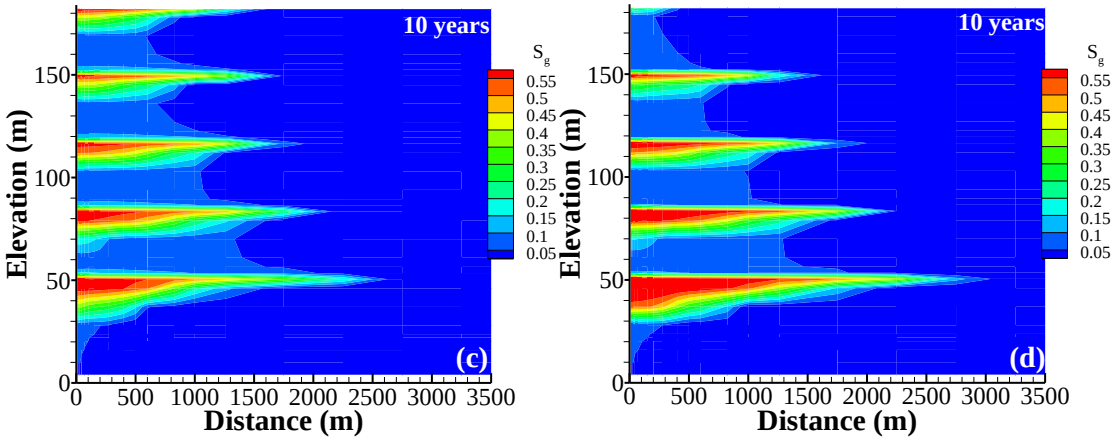

Fig. 4. The distribution of gas saturation after 10 years for different cases of capillary pressures: (a) Case 1; (b) Case 2; (c) Case 3; (d) Case 4.

CO_2 would slowly dissolve in the formation brine at the two-phase contact area after injection. Figure 5 presents the variation of dissolved CO_2 mass and dissolved CO_2 ratio for the four cases, and Table 3 lists the dissolved CO_2 ratio for different cases of capillary pressures at 10 years. Since the same amount of CO_2 has been injected, the variation trend of dissolved CO_2 ratio is the same as that of dissolved CO_2 mass. During the injection period, the dominant force for the CO_2 stream to displace the formation brine is the pressure buildup caused by injection, while the effect of capillary pressure can be neglected. As a result, the variation of capillary pressure does not have noticeable effects on the evolution of dissolved CO_2 mass during the first 2 years. It should be noted that the dissolved CO_2 mass in Case 2 is the least at 2 years. This can be explained by the distribution range of the CO_2 plume: as shown in Figure 2, the spread of CO_2 plume in Case 2 is the smallest at 2 years, which means the smallest two-phase contact area and the least amount of dissolved CO_2 mass.

During the post-injection period, the capillary pressure has significant influence on the dissolved CO_2 mass and ratio. In Case 1 without regard to capillary pressure, the amount of CO_2 dissolved in the formation brine is the highest. With increasing capillary pressure in the shale layers (from Case 2 to Case 4), dissolved CO_2 mass decreases correspondingly. The main reason is that the capillary pressure in the sand layers hinders the backflow of the formation brine while the capillary pressure in the shale layers limits the upward migration of the CO_2 plume, and thus the contact area between the CO_2 plume and the formation brine declines (Figure 4). As a result, the amount and ratio of CO_2 dissolved in the formation brine is reduced accordingly.

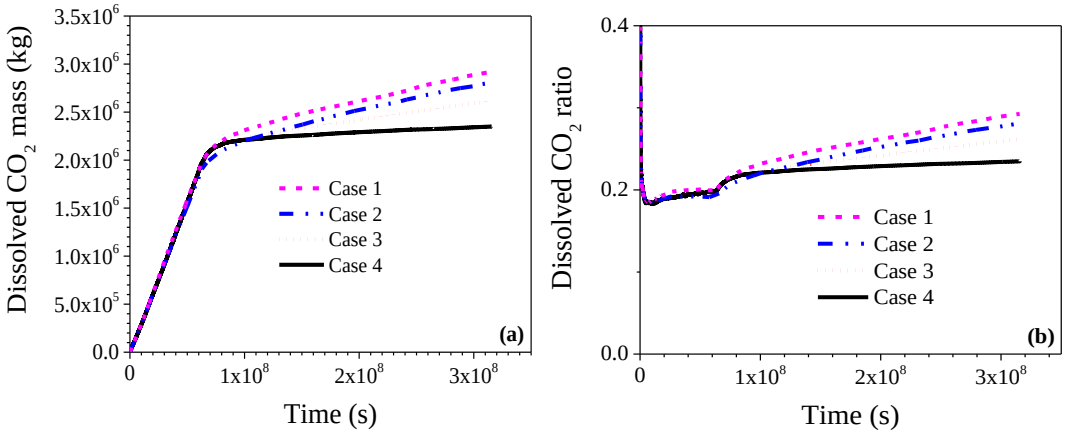

Fig. 5. The variation of (a) dissolved CO_2 mass and (b) dissolved CO_2 ratio for different cases of capillary pressures.

Table 3. Dissolvd CO_2 ratio for different cases of capillary pressures at 10 years.

	Case 1	Case 2	Case 3	Case 4
Dissolved CO_2 ratio	29.27%	28.10%	26.19%	23.48%

4. The effects of the N_2 and H_2S impurities

4.1 The variation of the spread of CO_2 plume

Figure 6 shows the distribution of the supercritical CO_2 plume after 2 years' injection for different injected mixtures, with the leading edge of the CO_2 plume highlighted. The horizontal migration distance of the CO_2 plume increases with increasing N_2 mole fraction during injection. For instance, when N_2 concentration is 10%, the leading edge of the CO_2 plume has reached about 3100 m after 2 years while it is only about 2200 m in the pure CO_2 case. Furthermore, CO_2 tends to accumulate under the impermeable caprock, especially at higher N_2 concentrations (Figures 6d and 6f). However, the effects of the H_2S impurity at all the investigated concentrations on the distribution range of the CO_2 plume can hardly be observed during the first 2 years.

Figure 7 compares the distribution of the supercritical plume after 10 years for different injected mixtures. It shows that the CO_2 plume under the shale layers continues migrating outwards from the injection well during the post-injection period, which could be ascribed to the relatively large capillary pressure (equals the values in Case4, Table 2). With increasing N_2 concentration, the horizontal migration distance increases considerably during the post-injection period. Specifically, the migration distance of the 10% N_2 case, about 5500 m, is almost 2 times of that of the pure CO_2 case (3000 m) at 10 years. On the contrary, with increasing H_2S concentration in the injected stream, the migration distance of the plume away from the injection well reduces a little bit after 10 years: when the co-injected CO_2 stream contains 10% H_2S, the migration distance of the CO_2 plume reduces to about 2800 m which is 200 m shorter than that of the pure CO_2 case.

The distinct evolution of the plume could be explained by the different properties of these species. The viscosity of N_2 is much smaller than that of CO_2 (Table 1). The inclusion of N_2 increases the mobility of the CO_2 plume, and thus the plume could displace the formation brine more effectively [40]. Furthermore, since the density of N_2 is lower than that of CO_2, the buoyance force experienced by the CO_2-N_2 mixture is larger than that of pure CO_2. As a consequence, with increasing N_2 concentration in the injected stream, more supercritical plume would have accumulated under the top caprock. On the contrary, the viscosity of H_2S is relatively larger than that of CO_2, and the migration rate of the CO_2 plume decreases consequently. Moreover, since the density of H_2S is slightly larger than that of CO_2, the amount of the CO_2-H_2S mixture that have migrated upward is supposed to decrease. However, since the solubility of H_2S is better than CO_2, most H_2S at the leading edge of the CO_2-H_2S plume has dissolved preferentially in the formation brine, which explains why the distributions of the gas saturation are similar at different H_2S concentrations in the injected stream. On the other hand, since the solubility of N_2 is much lower than that of CO_2, the effect of the N_2 impurity on the spread of the CO_2 plume is pretty significant.

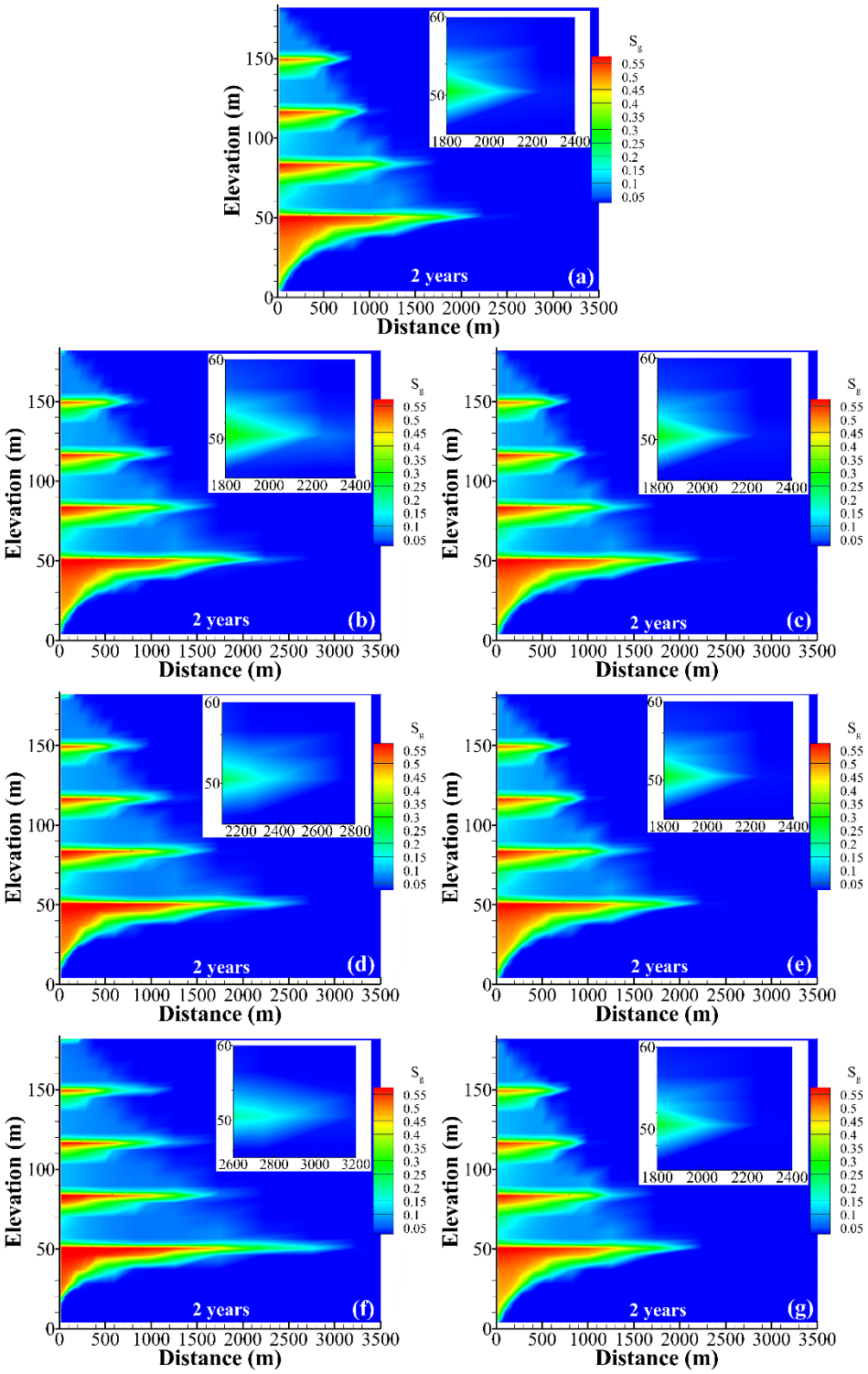

Fig. 6. The distribution of gas saturation after 2 years, (a) 100% CO_2, (b) 2% N_2, (c) 2% H_2S, (d) 5% N_2, (e) 5% H_2S, (f) 10% N_2, (g) 10% H_2S.

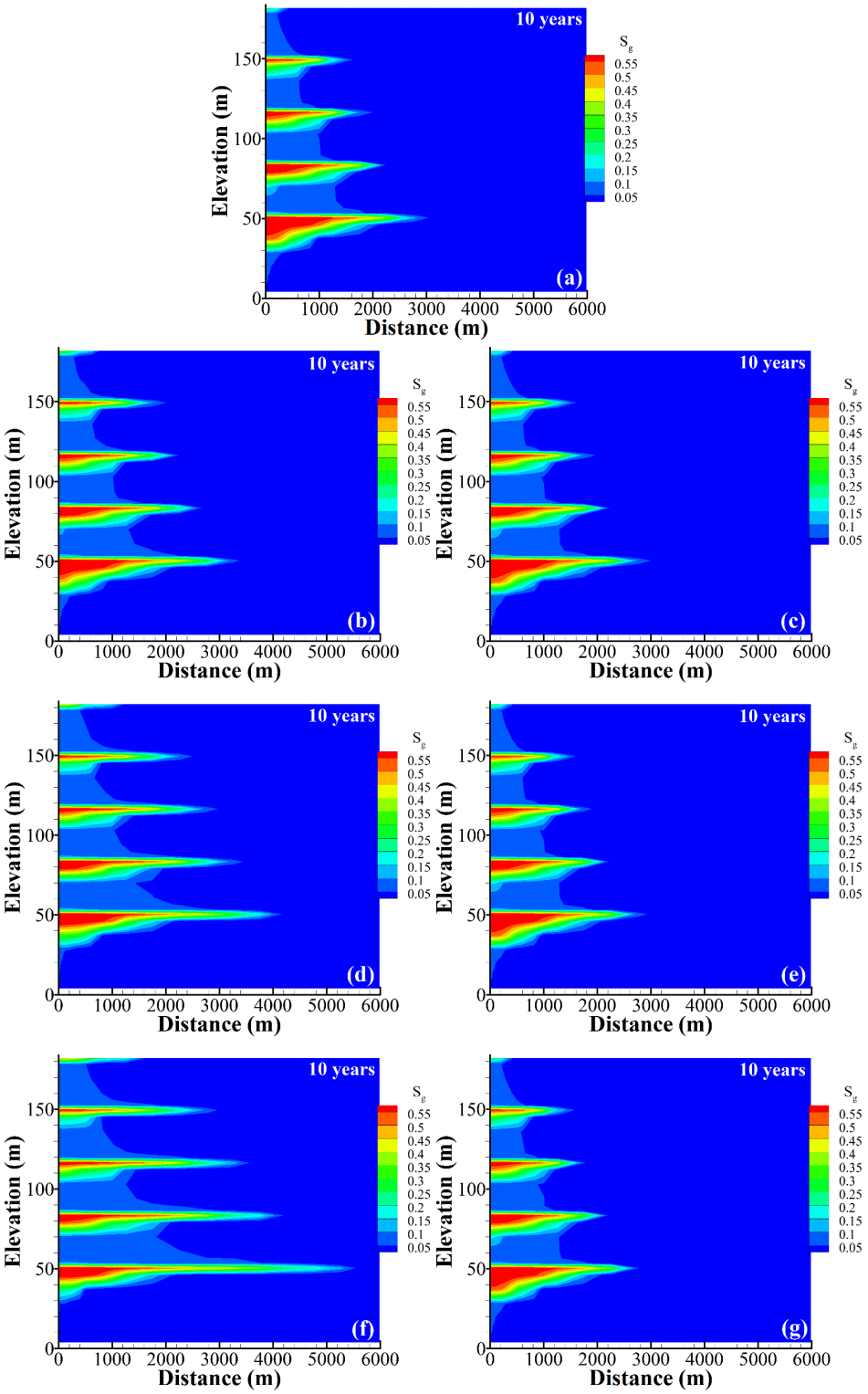

Fig. 7. The distribution of gas saturation after 10 years, (a) 100% CO_2, (b) 2% N_2, (c) 2% H_2S, (d) 5% N_2, (e) 5% H_2S, (f) 10% N_2, (g) 10% H_2S.

4.2 The partitioning phenomenon between CO_2 and the corresponding impurity

Figure 8 displays the distribution of the CO_2 concentration in the supercritical plume after 2 years, and Figure 9 presents the concentration distribution of the corresponding impurity (N_2 or H_2S) in the supercritical plume for different CO_2-impurity mixtures. When N_2 is co-injected with CO_2, higher concentration of CO_2 is found in the rear area of the advancing supercritical plume (Figures 8b, 8d and 8f), while N_2 dominates the

leading edge of the plume with much higher concentration than that in the injected mixture (Figures 9a, 9c and 9e). This is mainly because of the preferential dissolution of CO_2 compared with that of N_2. More CO_2 would dissolve in the formation brine at the leading edge of the plume, resulting in higher N_2 concentration in the gas phase. These results suggest that the partitioning phenomenon [40] could also take place in the layered formation. Due to the lower viscosity of N_2, the distribution range of the CO_2 concentration as well as the N_2 concentration in the gas phase increases with increasing N_2 concentration in the injected stream. Furthermore, since its density is smaller, the buoyancy force experienced by N_2 is larger, which is the main reason why a higher concentration of N_2 is mainly found under the caprock. In the case of the H_2S impurity, since its solubility is higher than CO_2, CO_2 with higher concentration is mainly distributed at the leading edge of the supercritical plume, while H_2S is mainly found behind the leading edge with concentrations not exceeding that in the injected stream. H_2S hardly reaches the caprock after 2 years, because the density and solubility of H_2S is higher than that of CO_2. Besides, when the impurity is at the same concentration in injected stream, N_2 mole fraction in the supercritical plume at 2 years is much higher than H_2S (Figure 9).

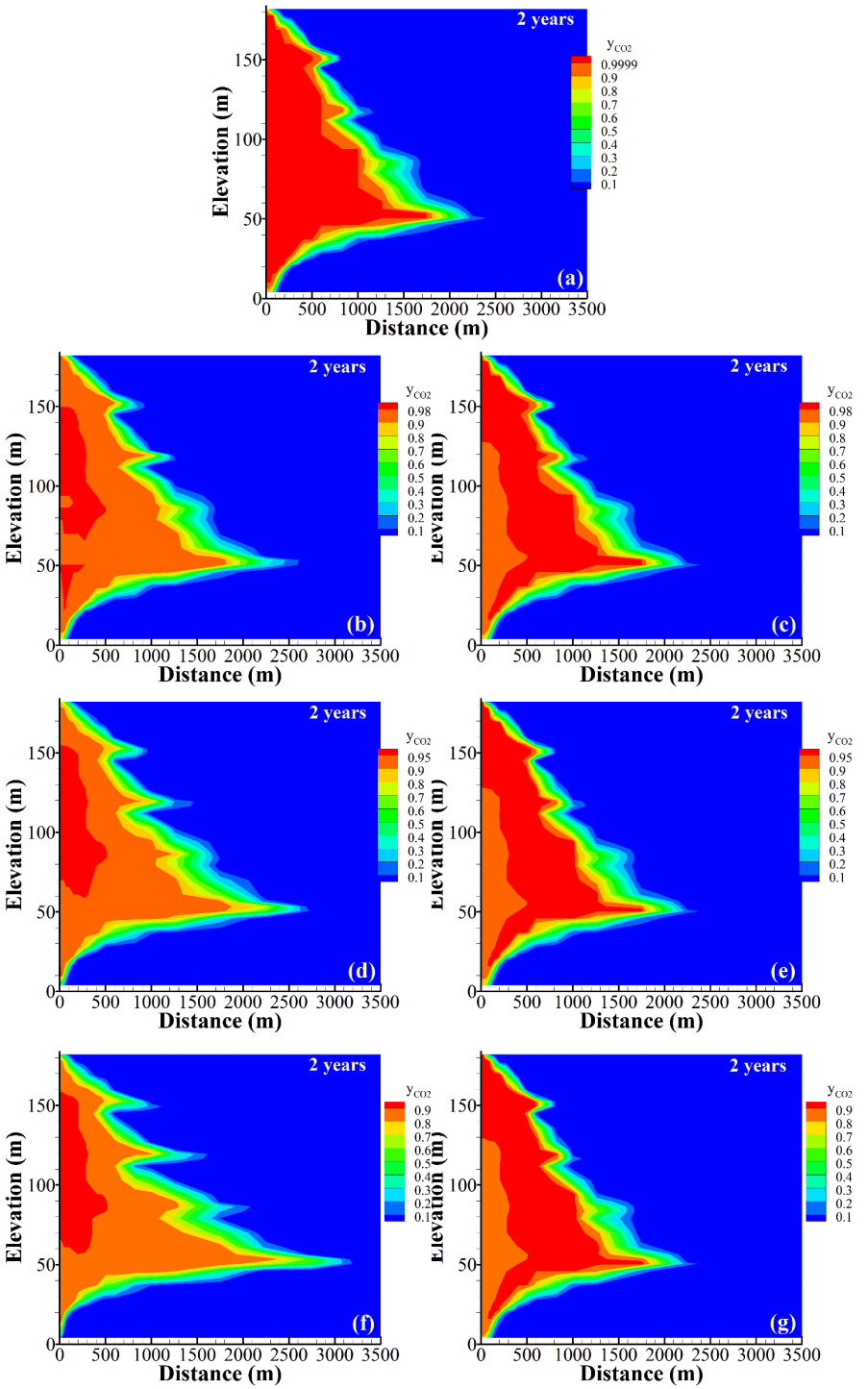

Fig. 8. The concentration distribution of CO_2 in the supercritical plume after 2 years, (a) 100% CO_2, (b) 2% N_2, (c) 2% H_2S, (d) 5% N_2, (e) 5% H_2S, (f) 10% N_2, (g) 10% H_2S.

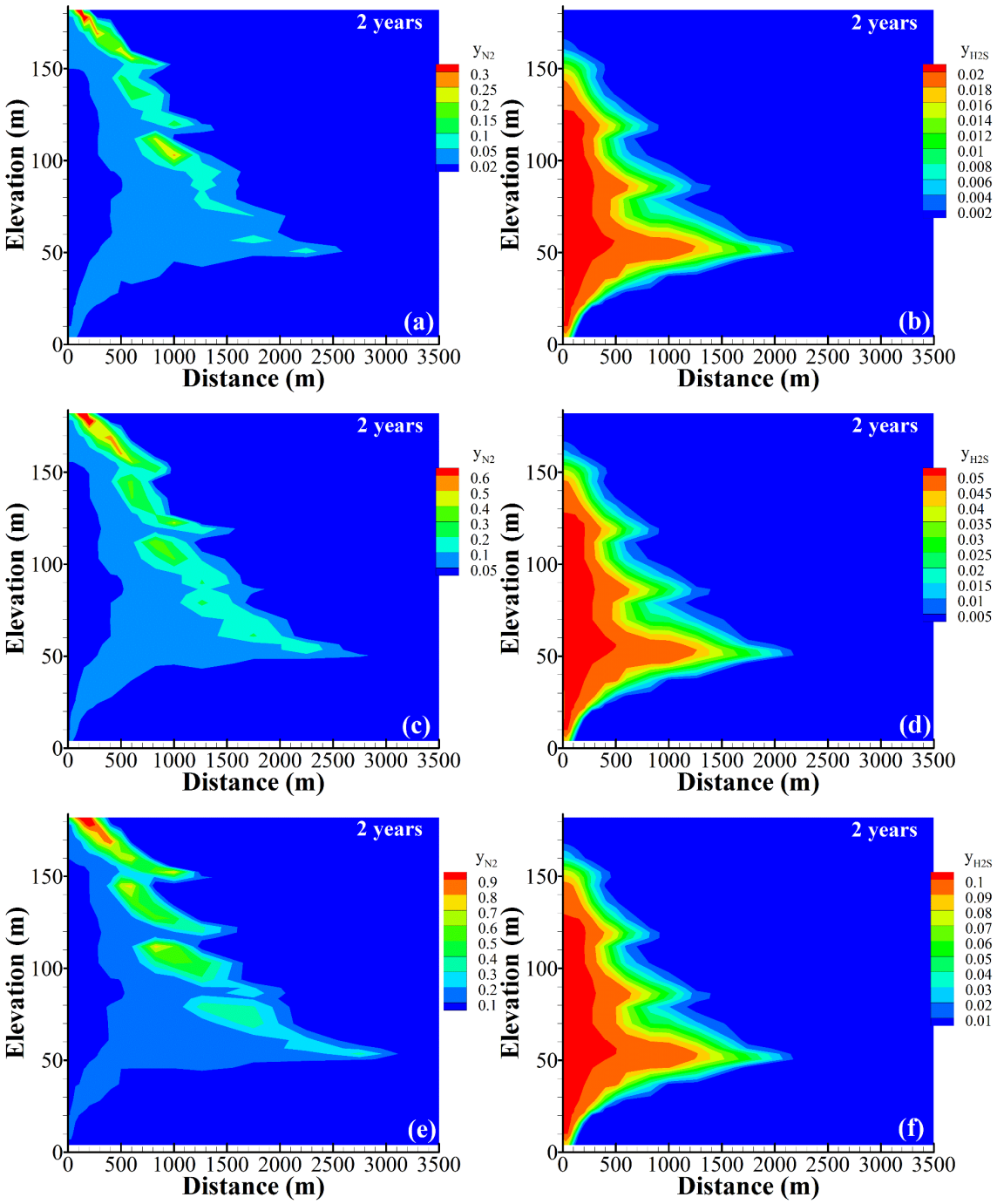

Fig. 9. The concentration distribution of impurity in the supercritical plume after 2 years, (a) 2% N_2, (b) 2% H_2S, (c) 5% N_2, (d) 5% H_2S, (e) 10% N_2, (f) 10% H_2S.

Figures 10 and 11 demonstrate the concentration distribution of CO_2 and the corresponding impurity (N_2 or H_2S) in the supercritical plume after 10 years, respectively. During the post-injection period, the plume continues migrating horizontally under the shale layers and displace the formation brine. Compared with the results at 2 years, the "viscous fingering" pattern of the CO_2 and impurity concentration is enhanced in the next 8 years.

Since the viscosity of N_2 is smaller than that of CO_2, the inclusion of N_2 would result in larger mobility of the CO_2-N_2 mixture, which means faster migration speed. As a result, with higher N_2 concentration in the injected stream, the horizontal migration distance of the CO_2-N_2 plume increases, leading to larger contact area between the formation brine and the plume. Consequently, more CO_2 would dissolve preferentially in

the brine due to its higher solubility, giving rise to a larger area of high N_2 concentration (>0.3). For instance, N_2 concentration at the leading edge of the displacing plume could reach more than 0.9 when the injected stream contains 10% N_2 (Figure 11e).

On the other hand, even though the viscosity of H_2S is much larger than that of CO_2, the horizontal migration distance of CO_2 or H_2S only decreases slightly with increasing H_2S concentration because of the preferential solubility of H_2S. After 10 years, there is still no H_2S that has arrived at the caprock resulted from the higher solubility of H_2S and the relatively larger density than that of CO_2. Moreover, H_2S concentration in the plume is basically the same as that in the injected stream.

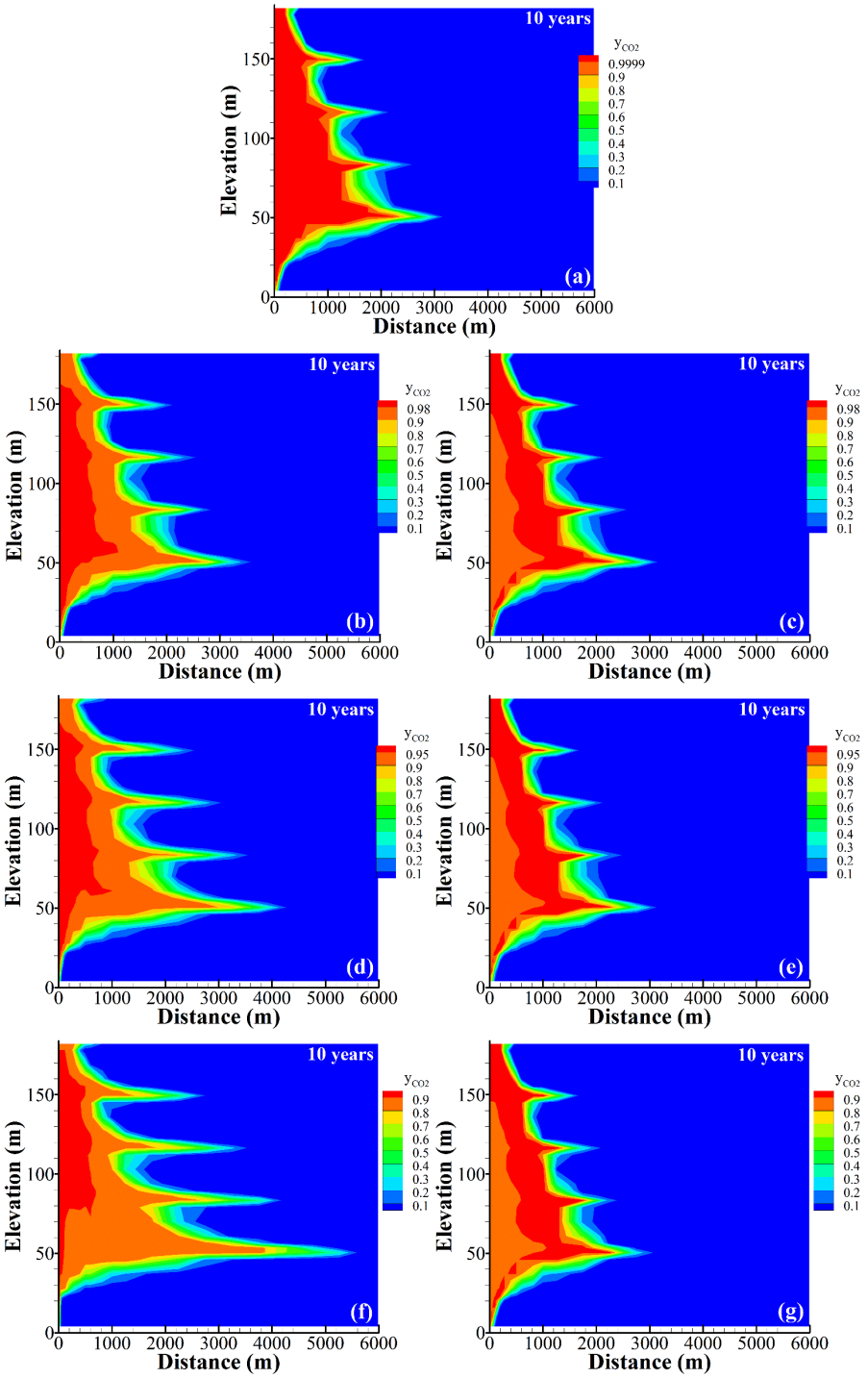

Fig. 10. The concentration distribution of CO_2 in the supercritical plume after 10 years, (a) 100% CO_2, (b) 2% N_2, (c) 2% H_2S, (d) 5% N_2, (e) 5% H_2S, (f) 10% N_2, (g) 10% H_2S.

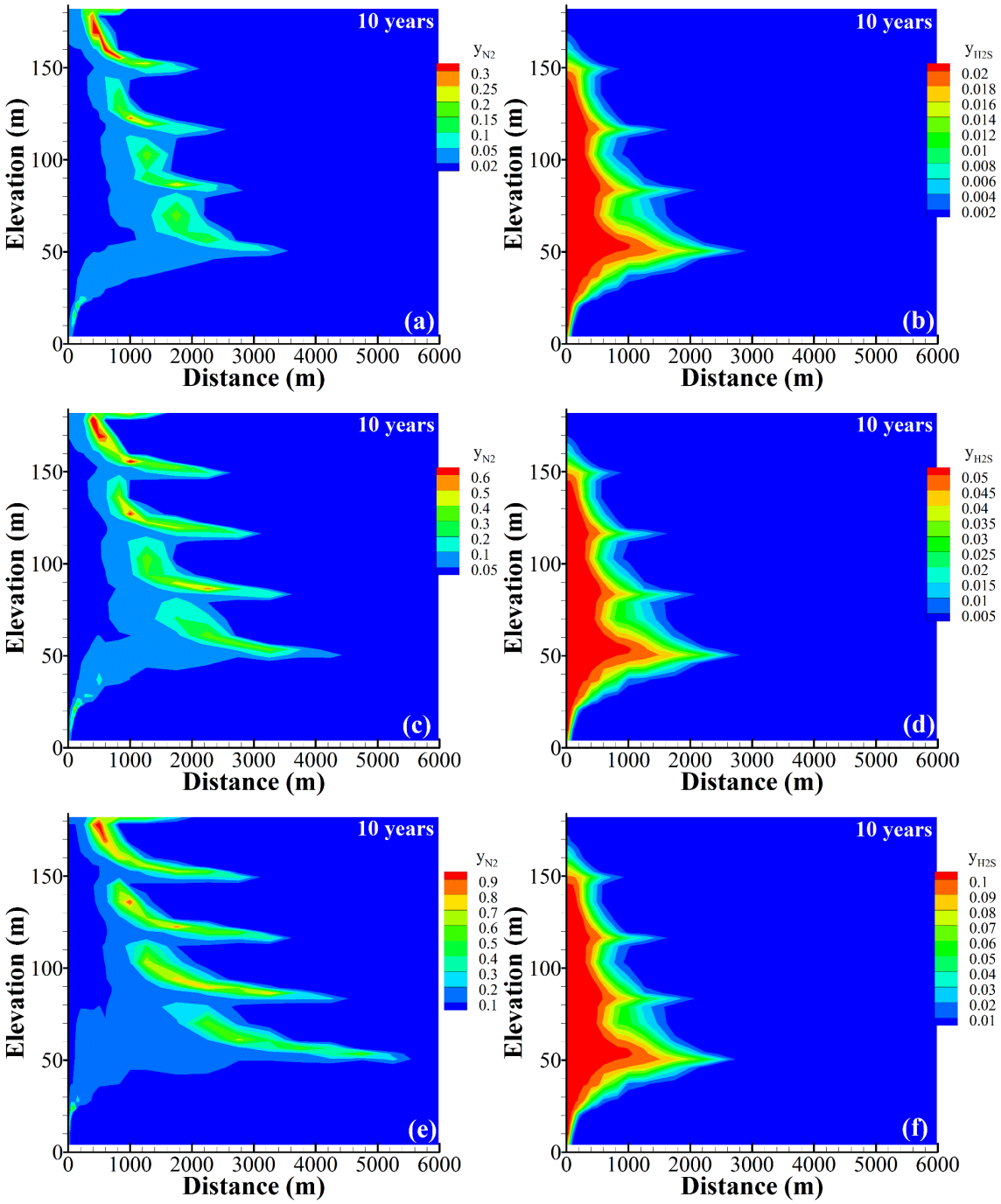

Fig. 11. The concentration distribution of impurity in the supercritical plume after 10 years, (a) 2% N_2, (b) 2% H_2S, (c) 5% N_2, (d) 5% H_2S, (e) 10% N_2, (f) 10% H_2S.

4.3 The variation of the dissolved CO_2 mass and ratio

Figure 12 presents the variations of the total injected CO_2 inventory, dissolved CO_2 mass and dissolved CO_2 ratio at different N_2 and H_2S concentrations, respectively. No matter what kind of impurity is co-injected, total amount of injected CO_2 decreases, which means a reduction of storage capacity of CO_2. Furthermore, with increasing impurity concentration, total injected CO_2 mass decreases accordingly (Figure 12a). Since N_2 is a non-condensable impurity, it reduces CO_2 capacity not only by replacement of CO_2, but also because it

does not compress to as great a degree as CO_2. As a result, the effect of N_2 on the reduction of total injected CO_2 mass is much stronger than that of H_2S.

The effect of N_2 on the dissolved CO_2 mass or ratio is opposite with that of H_2S. During the 2 years' injection period, neither the impurity species nor the impurity concentrations have made distinct difference in the dissolved CO_2 mass. During the post-injection period, however, the dissolved CO_2 mass increases considerably with increasing N_2 concentration in the injected CO_2 streams (Figure 12b). For example, although the 10% N_2 impurity cause the total injected CO_2 mass to reach its minimum (Figure 12a), it results in the maximum CO_2 mass dissolved. This is mainly due to the larger distribution range of the supercritical CO_2 plume with higher N_2 concentration (Figure 7), that is, the contact area between the CO_2 plume and the formation brine is larger, and thus more CO_2 dissolves. The effect of H_2S on the dissolved CO_2 mass is opposite with that of N_2 because of the shrinkage of the two-phase area (Figure 7).

As can be seen in Figure 12c, the proportion of dissolved CO_2 increases with increasing N_2 concentration while effects of H_2S concentration on the dissolved CO_2 ratio is limited. Table 4 lists the results of dissolved CO_2 ratio for different injected mixtures at 10 years. It can be seen that although the effects of H_2S is minor, the dissolved CO_2 ratio decreases slightly with increasing H_2S concentration. In general, the effect of N_2 is much more obvious than that of H_2S at the same concentration.

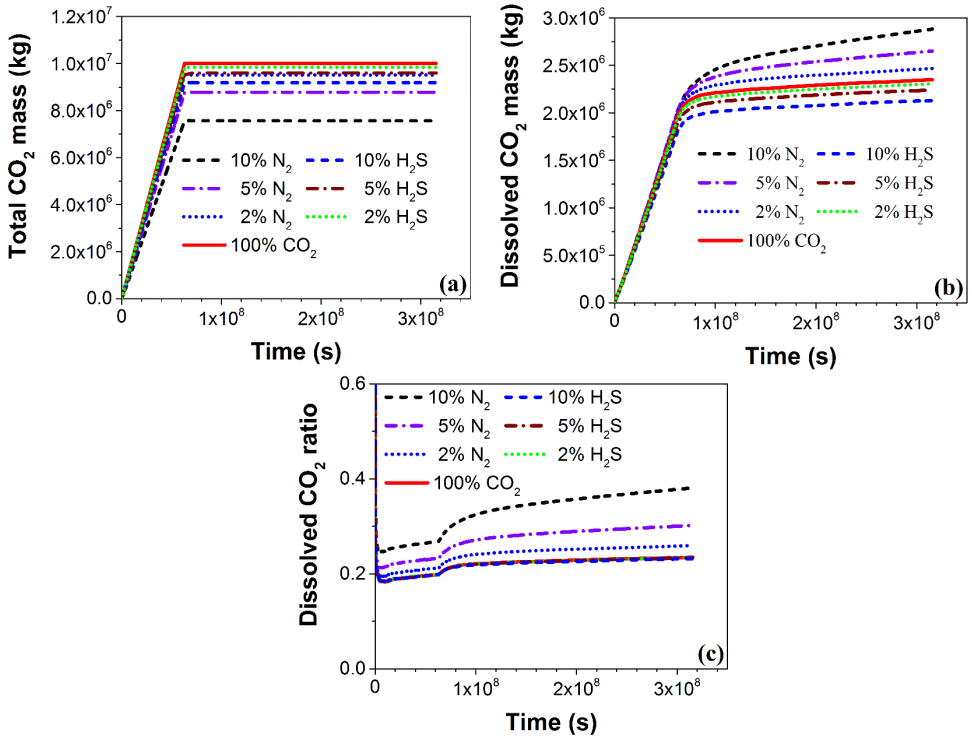

Fig. 12. The variations of (a) total CO_2 injected mass, (b) dissolved CO_2 mass and (c) dissolved CO_2 ratio, with N_2 or H_2S mole fractions varying from 0 to 10%.

Table 4. Dissolvd CO_2 ratio for different injected mixtures at 10 years.

	100% CO_2	2% N_2	5% N_2	10% N_2	2% H_2S	5% H_2S	10% H_2S
Dissolved CO_2 ratio	23.48%	25.94%	30.20%	38.09%	23.45%	23.37%	23.18%

5. Conclusions and future work

Most potential geological formations suitable for CO_2 storage are stratified. More importantly, non-CO_2 species are often co-injected with CO_2 to reduce costs in practical CCS projects. The properties of both the multilayered formations and the impurities would affect the security and effectiveness of CO_2 geological storage. In this study, the effects of N_2 and H_2S impurity on CO_2 geological storage in multilayered brine

formations were investigated numerically, by using the basic geological conditions in the Vest Field at Sleipner, Norway. This work firstly investigated the effects of capillary pressure in layered formations on the migration behviour of injected CO_2, in terms of the distribution of the supercritical CO_2 plume and the dissolved CO_2 mass/ratio. It was found that the capillary pressure did not make much difference during injection but the impact became much bigger during the post-injection period. The existence of the capillary pressure in the sand layers would hinder the backflow of the saline brine to some extent, resulting in smaller contact area between the plume and the brine. The capillary pressure in the shale layers, on the other hand, would limit the upward moving of the CO_2 plume. As a result, the dissolved CO_2 mass decreased with increasing capillary pressure.

When CO_2 was injected with the low-viscosity N_2 impurity, the horizontal migration distance of the CO_2-N_2 plume was longer when the concentration of the N_2 impurity was higher. In addition, the existence of the N_2 impurity enhanced the upward movement of the CO_2 plume due to its lower density. Consequently, the distribution range of the CO_2 plume was larger when N_2 concentration was higher. More CO_2 dissolved in the formation brine due to the larger contact area between the CO_2 plume and the formation fluids, and the dissolved CO_2 ratio was also larger. On the contrary, the effect of the H_2S impurity was opposite with that of the N_2 impurity: the lateral plume spread slightly decreased with increasing H_2S concentration as a result of the higher viscosity of H_2S than that of CO_2. The total dissolved CO_2 mass in the formation brine also decreased with increasing H_2S content. At the same impurity mole fraction, the effect of N_2 was much stronger than that of H_2S, partially because H_2S at the leading edge has preferentially dissolved in the formation brine. Because of the preferential dissolution of the other species in the saline brine, the leading edge of the plume was mainly made up of the species with relatively lower solubility, such as N_2 in the CO_2-N_2 mixture and CO_2 in the CO_2-H_2S mixture. Furthermore, the concentrations of the dominant species, *e.g.*, N_2, at the leading edge was much higher than that in the injected stream.

Our results could provide reference for the kinds and concentrations allowed in the impure CO_2 storage in layered formations. Take N_2 as an example: on the one hand, non-condensable N_2 decreases the storage capacity of CO_2, and increases the leakage risk of the injected plume because it leads to a larger distribution range of the plume both in the vertical and horizontal direction. On the other hand, the larger distribution range also results in an increase of the dissolved CO_2 mass and ratio. Furthermore, the partitioning phenomenon between CO_2 and N_2 could be used for devising monitoring procedures of possible leakage since N_2 flows ahead of CO_2 and would be detected earlier than CO_2 if leakage happens. Combined with the consideration of the effects of N_2 impurity on capture and transportation, the optimal range of N_2 impurity allowed in the injected stream could be determined.

In the present study, isothermal conditions were employed in the simulations for simplicity. In the future, the impact of temperature and multiple impurities will be taken into account since most impure CO_2 storage involves more than one kind of non-CO_2 species. In addition, fully three-dimensional simulations will be needed for practical storage scenarios.

Acknowledgement

This work was supported by the Fundamental Research Funds (51508110) and Natural Science Foundation of Guangdong Province (2016A030310341).

References

[1] Intergovernmental panel on climate change (IPCC). In: Metz B, Davidson O, de Coninck H, Loos M, Meyer LA, editors. IPCC special report on carbon dioxide capture and storage, New York: Cambridge University Press; 2005, p.53–72.

[2] Bachu S. CO_2 storage in geological media: role, means, status and barriers to deployment. Prog Energy Combust Sci 2008;34:254–73.

[3] Jiang X. A review of physical modelling and numerical simulation of long-term geological storage of CO_2. Appl Energy 2011;88(11):3557–66.

[4] Lindeberg E, Bergmo P, and Moen A. The long-term fate of CO_2 injected into an aquifer, paper G1-4, presented at Sixth International Conference on Greenhouse Gas Technologies (GHGT-6), Kyoto, Japan, October 1-4, 2002, p.468–73.
[5] Gupta N, Gupka NRO, Spitznogle G, Bollinger R, Bhattacharya I. Geologic storage and monitoring at American Electric Power's Mountaineer plant—what have we learned after one year of injection. In: Proceedings of 10th annual conference on carbon capture and sequestration, Pittsburgh, Pennsylvania, May 2–5, 2011.
[6] Rutqvist J. The geomechanics of CO_2 storage in deep sedimentary formations. Geotech Geol Eng 2012;30:525–51.
[7] Lu J, Kordi M, Hovorka SD, Meckel TA, Chrstopher CA. Reservoir characterization and complications for trapping mechanisms at Cranfield CO_2 injection site. Int J Greenhouse Gas Control 2013; 18:361–74.
[8] Zhang Z, Agarwal RK. Numerical simulation of CO_2 geological storage in saline aquifers – case study of Utsira formation. Int J Energy Environ 2014;5(1):23–34.
[9] Pruess K, García J, Kovscek T, Oldenburg C, Rutqvist J, Steefel C and Xu T. Intercomparison Builds Confidence in Numerical Simulation Models for Geologic Disposal. Laboratory Report LBNL-51813, Berkeley, CA 94720, December 2002.
[10] Pruess K, García J, Kovscek T, Oldenburg C, Rutqvist J, Steefel C and Xu T. Code intercomparison builds confidence in numerical simulation models for geologic disposal of CO_2. Energy 2004; 29: 1431–1444.
[11] Birkholzer JT, Zhou Q, Tsang C-F. Large-scale impact of CO_2 storage in deep saline aquifers: A sensitivity study on pressure response in stratified systems. Int J Greenhouse Gas Control 2009;3:181–94.
[12] Cihan A, Zhou Q, and Birkholzer JT. Analytical solutions for pressure perturbation and fluid leakage through aquitards and wells in multilayered aquifer systems. Water Resources Research 2011; 47: W10504 DOI:101029/2011WR010721.
[13] Cihan A, Birkholzer JT, Zhou Q. Pressure buildup and brine migration during CO_2 storage in multilayered aquifers. Groundwater 2013; 51(2):252–67.
[14] Li C, Wang Y, Guo C, Maggi F. Experimental and numerical analysis of reservoir performance for geological CO_2 storage in the Ordos Basin in China. Int J Greenhouse Gas Control 2016;45:216–32.
[15] Zhu Q, Zuo D, Zhang S, Zhang Y, Wang Y, Wang L. Simulation of geomechanical responses of reservoirs induced by CO_2 multilayer injection in the Shenhua CCS project, China. Int J Greenhouse Gas Control 2015;42:405–14.
[16] Baz H, Noureldin M, Allinson WG, Cinar YA. field-scale investigation of residual and dissolution trapping of CO_2 in a saline formation in Western Australia. Int J Greenhouse Gas Control 2016;46:86–9.
[17] Chang KW, Hesse MA, Nicot J-P. Reduction of lateral pressure propagation due to dissipation into ambient mudrocks during geological carbon dioxide storage. Water Resour Res 2013;49:2573–88.
[18] Liu B and Zhang Y. CO_2 modeling in a deep saline aquifer: A predictive uncertainty analysis using design of experiment. Environ Sci Technol 2011;45:3504–10.
[19] Bandilla KW, Celia MA, Elliot TR, Person M, Ellett KM, Rupp JA, et al. Modeling carbon sequestration in the Illinois Basin using a vertically-integrated approach. Comput Visual Sci 2012;15:39–51.
[20] Figueiredo B, Tsang C-F, Rutqvist J, Bensabat J, Niemi A. Coupled hydro-mechanical processes and fault reactivation induced by CO_2 Injection in a three-layer storage formation. Int J Greenhouse Gas Control 2015;39:432–48.
[21] Liu H, Hou Z, Were P, Gou Y, Sun X. Simulation of CO_2 plume movement in multilayered saline formations through multilayer injection technology in the Ordos Basin, China. Environ Earth Sci 2014;71:4447–62.
[22] Oh J, Kim K-Y, Han WS, Park E, Kim J-C. Migration behavior of supercritical and liquid CO_2 in a stratified system: Experiments and numerical simulations. Water Resour Res 2015;51:7937–58.
[23] Luo F, Xu R-N, Jiang P-X. Numerical investigation of the influence of vertical permeability heterogeneity in stratified formation and of injection/production well perforation placement on CO_2 geological storage with enhanced CH_4 recovery. Appl Energy 2013; 102:1314–23.
[24] Plampin MR, Lassen RN, Sakaki T, Porter ML, Pawar RJ, Jensen KH, et al. Heterogeneity-enhanced gas phase formation in shallow aquifers during leakage of CO_2-saturated water from geologic sequestration sites. Water Resour Res 2014; 50:9251–66.
[25] Kano Y, Ishido T. Numerical simulation on the long-term behavior of CO_2 injected into a deep saline aquifer composed of alternating layers. Energy Procedia 2011;4:4339–46.
[26] Cavanagh AJ, Haszeldine RS. The Sleipner storage site: Capillary flow modeling of a layered CO_2 plume requires fractured shale barriers within the Utsira Formation. Int J Greenhouse Gas Control 2014;21:101–12.
[27] Sung R-T, Li M-H, Dong J-J, Lin AT-S, Hsu S-K, Wang C-Y et al. Numerical assessment of CO_2 geological sequestration in sloping and layered heterogeneous formations: A case study from Taiwan. Int J Greenhouse Gas Control 2014; 20:168–79.

[28] Li D and Jiang X. A numerical study of the impurity effects of nitrogen and sulfur dioxide on the solubility trapping of carbon dioxide geological storage. Appl Energy 2014;128:60–74.
[29] De Silva GPD, Ranjith PG, Perera MSA. Geochemical aspects of CO 2 sequestration in deep saline aquifers: A review. Fuel 2015; 155: 128–43.
[30] Hassanzadeh H, Pooladi-Darvish M, Keith DW. Accelerating CO_2 dissolution in saline aquifers for geological storage – mechanistic and sensitivity studies. Energy Fuels 2009;23:3328–36.
[31] Agartan E, Trevisan L, Cihan A, Birkholzer J, Zhou Q, Illangasekare TH. Experimental study on effects of geologic heterogeneity in enhancing dissolution trapping of supercritical CO_2. Water Resour Res 2015;51:1635–48.
[32] Liu H, Shao YJ. Predictions of the impurities in the CO_2 stream of an oxy-coal combustion plant. Appl Energy 2010;87(10):3162–70.
[33] Li HL, Jakobsen JP, Wilhelmsen Ø, Yan JY. PVTxy properties of CO_2 mixtures relevant for CO_2 capture, transport and storage: review of available experimental data and theoretical models. Appl Energy 2011;88:3567–79.
[34] Wang J, Ryan D, Anthony EJ, Wigston A. Effects of impurities on geological storage of CO_2. Report for IEA GHG, 2011.
[35] Li H, Yan J. Evaluating cubic equations of state for calculation of vapor–liquid equilibrium of CO_2 and CO_2-mixtures for CO_2 capture and storage processes.Appl Energy 2009;86(6):826–36.
[36] Li H, Yan J. Impacts of equations of state (EOS) and impurities on the volume calculation of CO_2 mixtures in the applications of CO_2 capture and storage (CCS) processes. Appl Energy 2009;86(12):2760–70.
[37] Li HL, Wilhelmsen Ø, Lv YX, Wang WL, Yan JY. Viscosities, thermal conductivities and diffusion coefficients of CO_2 mixtures: review of experimental data and theoretical models. Int J Greenhouse Gas Control 2011;5:1119–39.
[38] Ji XY, Zhu C. Predicting possible effects of H_2S impurity on CO_2 transportation and geological storage. Environ Sci Technol 2013;47:55–62.
[39] Wei N, Li XC, Wang Y, Zhu QL, Liu SN, Liu NZ, et al. Geochemical impact of aquifer storage for impure CO_2 containing O_2 and N_2: Tongliao field experiment. Appl Energy 2015;145:198–210.
[40] Li D, Jiang X. Numerical investigation of the partitioning phenomenon of carbon dioxide and multiple impurities in deep saline aquifers. Appl Energy 2017;185:1411–23.
[41] Computer Modelling Group (CMG). User's Guide-GEM: Advanced Compositional Reservoir Simulator. Version 2012. Computer Modelling Group Ltd, Calgary, AB, Canada, 2012.
[42] Van Genuchten MTH. A closed-form equation for predicting the hydraulic conductivity of unsaturated soils. Soil Sci Soc 1980; 44: 892–8.
[43] de Visser E, Hendriks C, Barrio M, Mølnvik MJ, de Koeijer G, Liljemark S, et al. Dynamis CO_2 quality recommendations. Int J Greenhouse Gas Control 2008;2:478–84.
[44] Arts R, Eiken O, Chadwick A, Zweigel P, van der Meer LGH, Zinszner B. Monitoring of CO_2 injected at Sleipner using time-lapse seismic data. Energy 2004;29:1383–92.
[45] Bickle M, Chadwick RA, Huppert HE, Hallworth M, Lyle S. Modelling CO_2 accumulation at Sleipner: implications for underground carbon storage. Earth Planet Sc Lett 2007;255:164–76.
[46] Chadwick RA, Arts R, Bentham M, Eiken O, Holloway S, Kirby GA, et al. Review of monitoring issues and technologies associated with the long-term underground storage of carbon dioxide. J Geol Soc London, Special Publications 2009;313:257–75.
[47] Cavanagh A. Benchmark calibration and prediction of the Sleipner CO_2 plume from 2006 to 2012. Energy Procedia 2013;37:3529–45.